JMEPEG (2023) 32:9814–9824
https://doi.org/10.1007/s11665-023-08244-2

1059-9495/$19.00

TECHNICAL ARTICLE

Microstructural Characterization of Novel ZrO_2 Dispersion-Strengthened 9Cr Steel by Spark Plasma Sintering

K.G. Raghavendra, Arup Dasgupta, N.S. Karthiselva, K. Jayasankar, and Srinivasa Rao Bakshi

Submitted: 12 January 2023 / Revised: 27 March 2023 / Accepted: 11 April 2023 / Published online: 8 May 2023

Technologically important Oxide Dispersion-Strengthened steels are synthesized using ZrO_2 as a dispersion strengthener instead of conventionally used Y_2O_3. Powder metallurgical route followed by spark plasma sintering is adopted for synthesizing the material. Detailed microstructural characterization revealed a fine-grained microstructure with finer dispersoids in as-sintered and normalized condition. The stable microstructure is found to be retained even after subjecting the samples at 973 K for as long as 1000 h for long-term thermal aging trials, indicating at a possible superiority of this material over the conventional Oxide Dispersion-Strengthened steels. The yield strength is calculated by making use of microstructural parameters and predictive models, both of which shown a good agreement. Mechanical property analysis through hardness measurements was correlated with microstructural observations and compared with the conventional Oxide Dispersion-Strengthened steels. The collective results indicate ZrO_2 as a potential alternate dispersoid for strengthening steel and future scope for vast exploration.

Keywords ZrO_2, electron microscopy, microstructure, oxide dispersion strengthening, steel, sintering

1. Introduction

The development of advanced materials for high-technology applications is an ever-active domain with consistent growth and breakthroughs. Modern technologies, including clean energy sector, require materials which have specific properties for their intended applications and are being constantly looked for (Ref 1–6). Oxide Dispersion-Strengthened (ODS) steels are one such class of materials with enhanced creep strength at elevated temperatures up to 973 K, which are being developed as a core structural material for next-generation Fast Breeder Reactors (FBRs) (Ref 1, 7). In particular, ODS alloys are being developed as clad tube, which houses the nuclear fuel pellets. Primary requirement for these ODS alloys is the superior creep strength at operating temperatures which could be as high as 923–973 K and additionally, these alloys also need to have superior void swelling resistance and sustained high temperature mechanical strength (Ref 1, 7, 8). While Austenitic steels are currently being used as nuclear structural materials in critical components, ferritic steels are increasingly being considered for next-generation sodium-cooled FBRs due to their open body-centered cubic (bcc) structure, which is known to provide superior void swelling resistance compared to their austenitic counterparts. However, high temperature creep strength is an issue with ferritic steels, leading to their restricted usage at higher temperatures. This issue can be resolved by addition of fine ceramic dispersions, as in the case of ODS alloys, wherein the ceramic dispersions block the mobile dislocations to enhance their high temperature creep strength. The addition of ceramic dispersions, however, cannot be done through conventional melting route owing to the density differences between the alloy and dispersoid and have to be carried out through powder metallurgical/ball milling route. Although there are persistent explorations on alternate methods of ODS alloy synthesis (Ref 9–13), the powder metallurgy synthesis is still extensively used and well-established. The most common dispersoid used in ODS steels is Y_2O_3, and it has been studied widely. However, the limitation with Y_2O_3 is its coarsening at elevated temperatures during consolidation of ball milled powders which will affect the mechanical properties of ODS steel and it is a serious limitation in its applications (Ref 14). This problem could be overcome by adding Ti to Y_2O_3 to facilitate the formation of complex oxides in the form of $Y_2Ti_2O_7$ and $YTiO_5$, which are finer and stable and subject of wide research (Ref 15, 16). Another approach to overcome this issue is to look for the alternate oxides which have better dispersoid refinement properties and lower coarsening kinetics. Owing to its huge potential, this approach is capable of

K.G. Raghavendra, Department of Physics, Manipal Institute of Technology, Manipal Academy of Higher Education, Manipal, Karnataka 576104, India; and Physical Metallurgy Division, Metallurgy and Materials Group, Indira Gandhi Centre for Atomic Research, HBNI, Kalpakkam, Tamilnadu 603102, India; **Arup Dasgupta**, Physical Metallurgy Division, Metallurgy and Materials Group, Indira Gandhi Centre for Atomic Research, HBNI, Kalpakkam, Tamilnadu 603102, India; **N.S. Karthiselva** and **Srinivasa Rao Bakshi**, Department of Metallurgical and Materials Engineering, Indian Institute of Technology, Madras, Chennai, Tamil Nadu 600036, India; and **K. Jayasankar**, Materials Science & Technology Division, CSIR-National Institute for Interdisciplinary Science and Technology, Thiruvananthapuram, Kerala 695019, India. Contact e-mail: raghavendra.kg@manipal.edu.

producing viable outcomes and possibly solve the issue we face with dispersoid coarsening.

Alternate dispersoids are being investigated in the recent past for their strengthening effects in alloys, specifically at high temperatures. In addition, since the irradiation response is a vital factor in nuclear structural materials, alternative dispersoids with varying chemistry are of significant interest. This is because, the evolution of the nano-sized oxides under irradiation depends on the chemical composition of the oxides (Ref 17), and hence, there could be novel dispersoids with better irradiation response than the widely used Y_2O_3/Y_2O_3-Ti complexes. Few of the reports on alternate dispersoids specific to ODS alloys include using ZrO_2, HfO_2, CeO_2, La_2O_3 and even the ex situ synthesized $Y_2Ti_2O_7$ and $Y_4Zr_3O_{12}$ as a dispersion strengthener (Ref 18–24). In one of the reports, Hoffmann et al. (Ref 22) investigated the mechanical properties of various steels strengthened by dispersoids, namely ZrO_2, CeO_2, HfO_2 and La_2O_3 and reported superior mechanical properties with ZrO_2 and La_2O_3 and proved the merit of exploring alternate dispersoids. This exploration is also fueled with the geopolitical scenarios with non-uniform distribution of rare earths in various parts of world as reported by Pasebani et al. (Ref 20, 21), who explored La_2O_3 as an alternate dispersoid owing to its abundance in USA and reported promising results with it.

Lately, there has been a growing interest in utilizing the advantages of ZrO_2 as a dispersion strengthener due to its smaller unit cell structure and relatively lower absorption cross section for fast neutrons. (Ref 22, 25–29). The ZrO_2 has a monoclinic structure which is stable up to 1443 K with no intermediate phase transformations and also has a smaller unit cell structure with 12 atoms in its unit cell (mP12). The smaller unit cell structure is predicted to be beneficial in retaining its crystal structure during the mechanical milling process. In addition to the direct addition of ZrO_2 in to the steel matrix as reported in literatures, the Zr is also reported as a potential microalloying element to produce ODS steels with favorable mechanical performance, irradiation response (Ref 30–32) and to refine the dispersoid sizes and optimize nanoprecipitate dispersion characteristics (Ref 33–35). A good combination of tensile strength and ductility is reported by Zhou et al. where Zr is used as a microalloying element and ZrO_2 and complex Y-Zr-O oxide formation is reported (Ref 36). There are promising results on irradiation response of Zr added ODS steel with formation of Y-Zr-O precipitates, which are superior to Y-Al-O and even Y-Ti-O precipitates (Ref 32, 37). Promising irradiation response with less susceptibility to radiation hardening is also reported in an austenitic ODS steel strengthened by Y_2O_3-ZrO_2 (Ref 38), further emphasizing the importance of exploring alternate dispersoids such as ZrO_2. With indications of being a potential strengthener, the ZrO_2 needs to be explored more in order to exploit its full potential.

Conventionally the ODS alloys are prepared through powder metallurgy route followed by consolidation through hot isostatic pressing (HIP) or spark plasma sintering (SPS). Generally, this process is followed with a heat treatment sequence for achieving the desired microstructure of the material. It is known that these processing steps play a huge role in final microstructure developed, and hence, it becomes essential to understand the process of microstructure evolution. We have previously reported (Ref 26) the microstructure development in the ball milled powder, and, in this article, we report the microstructure and mechanical property analysis of a SPS'd ZrO_2 dispersion-strengthened 9Cr steel alloy. The choice of 9Cr variant steel as base matrix is driven by the fact that it is at a higher technology readiness level for fuel cladding tubes among all the candidate steels, and hence, it is one of the closest materials to actual industrial implementation phase (Ref 39). The objective of the current study is to demonstrate the feasibility of using ZrO_2 as a dispersion strengthener in 9Cr steel system and to evaluate its high temperature microstructure and mechanical properties. In order to accomplish this, an extensive study of the material is performed by utilizing electron microscopy and allied techniques to evaluate its microstructure and the results of the analysis are presented in this report.

2. Experimental

The synthesis of 9Cr ODS steel powder with 0.35 wt.% ZrO_2 is carried out in a planetary ball mill in an Ar atmosphere. Detailed chemistry of the initial powder is given in Table 1. The particulars of the synthesis, its microstructure and microchemical characterization and the optimization of milling conditions are reported previously (Ref 26, 28, 29). The optimized milling duration was reported to be 100 h, and the synthesized powders at the optimal milling conditions had a grain size range of 1–20 μm (Ref 26). The process of consolidating the milled powders was carried out using Dr. Sinter make Spark Plasma Sintering (SPS) instrument at a temperature of 1323 K and a pressure of 50 MPa, applied for 10 min. The applied heating rate was 50 °C/min, and the samples were 20 mm in diameter and 5 mm height. The choice of Temperature and Pressure was based on the literature reports from similar systems (Ref 40–47) by considering a high relative density and reduced porosity. The density of the consolidated specimens is calculated by Archimedes principle. Five specimens were cut from various regions of the consolidated material and used for the measurements. The conventional Normalizing and Tempering (N&T) treatment is carried out for about 1 h each at temperatures of 1323 and 1023 K in a muffle furnace, to homogenize the microstructure (Ref 39). Further, the long-term annealing of the N&T sample at 973 K is carried out for 400 and 1000 h, to understand the microstructural stability. The heating rate was maintained at $\sim$ 20 °C/min to reach the desired temperature. Surface microstructure of the specimens was analyzed through a FEI make Dual Beam Helios NanoLab-600i FEG–Scanning Electron Microscope (SEM) attached with an EDAX make Apollo X Silicon Drift Detector for Energy-Dispersive Spectroscopy (EDS) microanalysis. The grain structure was examined through an EDAX make Electron Backscattering Diffraction (EBSD) detector, attached with the SEM. A 200 kV Philips make CM-200 Transmission Electron microscope (TEM) attached with TVIPS make 2 $\times$ 2 K CCD camera was used to observe the microstructure. The mechanical hardness of the material was analyzed through Vickers hardness measurements with a 50 g load. A total of 20 measurements were performed for each sample, before reporting the average hardness value.

3. Results and Discussion

3.1 Density Measurement of Consolidated 9Cr ZrO_2 ODS Steel

The density of the consolidated specimen was calculated by Archimedes principle, as explained previously. The objective

Table 1 Chemical composition of the 9 Cr steel powder (Wt.%)

Fe	Cr	W	Mn	Ni	Si	P	C	S	O	N	Al
Bal	9.2	2.25	0.026	0.01	0.02	0.004	0.015	0.001	0.015	0.002	< 0.005

Table 2 Measured densities of 9 Cr ZrO_2 ODS

Specimen no	Relative density, %
1	92.42
2	94.80
3	95.67
4	93.96
5	94.17
Average	94.20

here was to calculate an overall average density of the sample and look for any possible inhomogeneity. The measured values of the specimens taken from various regions of the consolidated sample are tabulated in Table 2.

It can be observed from the above table that relative densities vary between ~ 92 and 96% with an average of ~ 94%. This indicates a uniform distribution of porosity and less probability of local inhomogeneity within the sample during consolidation. It also indicates that the sintering parameters are optimum to achieve the higher efficiency of thermal energy, which aided in faster diffusion and compaction. For further analysis, sample region with relatively high density was used.

3.2 Microstructural Analysis of as-SPS'd 9Cr ZrO_2 ODS Steel

Typical microstructure of the as-SPS steel is shown in Fig. 1(a). The specimen showed a fairly homogeneous distribution of grains and pores, and the grain features were clearly smaller. The overall distribution of pores is about ~ 50–80 nm size and exhibits a tendency to network along grain boundaries. Figure 1(b) shows the EBSD Inverse Pole Figure (IPF) of the same sample at a relatively lower magnification superimposed with grain boundary, after the standard post processing to assign average orientation to non-indexed points based on its surrounding pixels. It reveals equiaxed grain morphology with nearly similar grain shape/size. Grain boundaries with a misorientation 5–15° and > 15° were identified as high angle and low angle boundaries, respectively. The average grain size was measured to be 0.8 ± 0.3 μm. The colors denote the type of crystallographic plane aligned with the sample surface, and the myriad of colors denotes an essential random type of texture in the specimen. It could be argued here that grain growth kinetics is restricted in the process due to minimum holding time at high temperature during consolidation through SPS and subsequent pinning effect of ZrO_2 dispersoids.

Figure 2 shows the TEM microstructure of the as-SPS'd 9Cr ZrO_2 ODS steel. The diffraction contrast from Fig. 2(a) reveals a microstructure, in which some fine faceted ferrite grains with high dislocations density are seen. This is an indicative of retention of strain even after consolidation. In addition to it, few

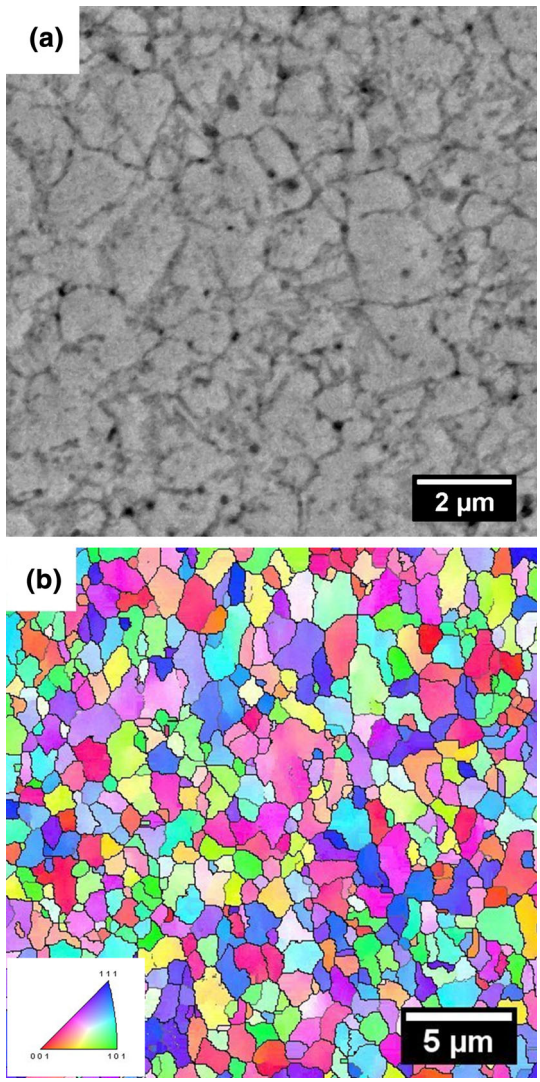

Fig. 1 Microstructure of as-SPS 9Cr ZrO_2 ODS steel (a) Secondary Electron micrograph (b) Inverse Pole Figure map showing the equiaxed grain structure

larger precipitates are also seen from this figure. TEM investigation at higher magnification revealed the presence of uniform distribution of nano-sized dispersoids inside the grains as shown in Fig. 2(b) with inset showing the selected area electron diffraction (SAED) patterns with unique reflections from ZrO_2 highlighted with an arrow mark. It is observed from further analysis that these nano-sized dispersoids in the matrix after consolidation through SPS retain their fine size ranging between 2 and 12 nm. The size distribution here is in close agreement with the reported values of < 5 nm, for the same system in as milled condition (Ref 26). The results are also in

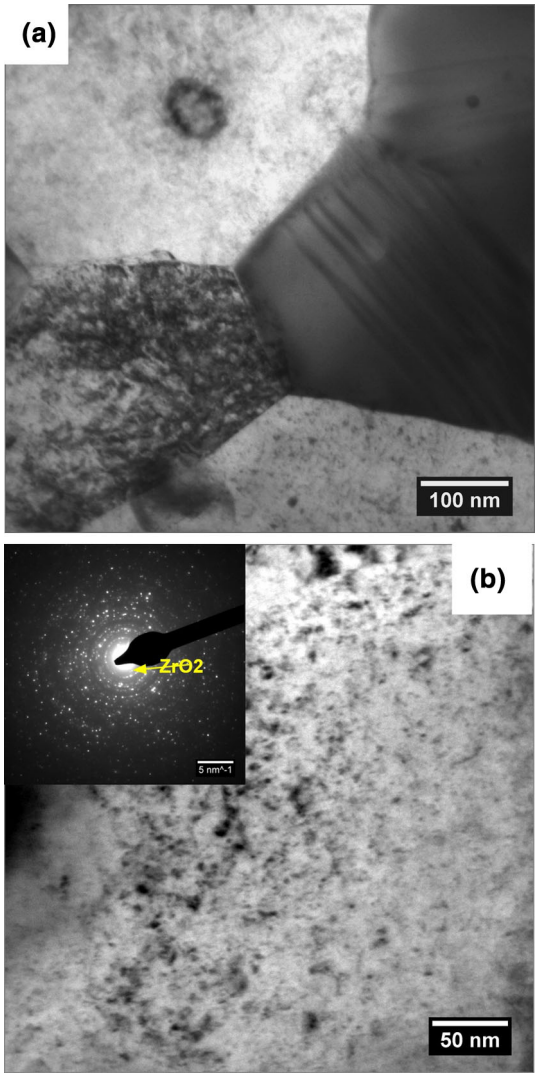

Fig. 2 Transmission Electron Micrographs of as SPS 9Cr ZrO_2 ODS steel showing (a) microstructure with grains and precipitate and (b) Grain dispersed with finer dispersoids with inset showing the SAED pattern

line with the reported values in the literature for similar ODS systems consolidated through SPS. Meza et al. (Ref 48) have reported a size distribution of 2—22 nm for a 14Cr-Y_2O_3 ODS system which reduced to 2—12 nm with Boron addition and the average size decreased from 8.11 to 4.26 nm. In another study, Li et al. (Ref 49) showed an average dispersoid size of 7 nm with a size distribution of 2–22 nm in a 14Cr-ODS system, just after SPS, with majority of dispersoids possessing a size less than 10 nm. The superiority of SPS in terms of its short residence time compared to other consolidation techniques is evident here, as we could retain the fine structure of the dispersoids without any detrimental increase in size for the nano-dispersoids. Further, owing to this strained inhomogeneous microstructure as observed through TEM, it is concluded that this issue needs to be addressed before carrying out further investigation. Accordingly, the samples were normalized at 1323 K for 1 h followed by a tempering treatment at 1023 K for 1 h to homogenize the microstructure. In addition to that, to assess the long-term effects on high temperature exposure, the samples were treated at 973 K for 400 and 1000 h durations and subsequently characterized. The results of the same are discussed in subsequent sections.

3.3 Effect of High-Temperature Treatment on 9Cr ZrO_2 ODS Steel—Normalizing & Tempering and Aging Studies

3.3.1 Microstructural Analysis by Scanning Electron Microscopy and Electron Backscatter Diffraction. Figure 3(a) shows the EBSD crystal orientation map of N&T 9Cr ZrO_2 ODS steel. A similar microstructure in comparison with as SPS condition is observed here with an average grain size of $\sim 1 \pm 0.4$ μm, also exhibiting a random orientation. Further, the long-term thermal treatment of the N&T sample at 973 K is carried out for 400 and 1000 h, to understand the microstructural stability as discussed previously. The temperature chosen here is typical at the service condition of reactor operation, and hence, this study is expected to provide vital information about the material microstructure. Figure 3(b) and (c) shows the corresponding EBSD crystal orientation map for the 400 and 1000 h aged samples, respectively. The grain size distribution is quantified, and analysis is carried out and shown in Fig. 3(d). All three samples (N&T, N&T + 400 h aged and N&T + 1000 h aged) show a uniform size distribution with little shift in peak grain size toward higher values. The average value of $\sim 1.0 \pm 0.4$ μm, 1.1 ± 0.5 μm and 1.3 ± 0.6 μm was observed for N&T, 400 and 1000 h samples, respectively. The grain size distribution of as SPS sample is also been included in the graph and shown a value of $\sim 0.8 \pm 0.3$ μm. The finer grain size distribution is a characteristic of SPS'd steels, and similar values are reported for other 9Cr ODS system in the literature (Ref 50). In addition, the retention of fine grain size after aging is also in line with previously reported studies (Ref 51, 52), where a grain size of 1.9, 2.2 and 2.5 μm is reported after SPS, aging at 973 K for 5000 and 10000 h, respectively. The finer grain sizes even after prolonged annealing are indicating the superior stability of the microstructure in this time–temperature domain which could be attributed due to the presence of hasten pinning effect by uniformly distributed fine dispersoids even at 973 K.

The superior stability of the microstructure with no substantial grain growth and saturated strain during this prolonged annealing is believed to be arising also from the stability of the dispersoids at this time–temperature domain. The dispersoids are known to effectively pin the grain boundaries thus inhibiting their growth is believed to be the case here, which is also in line with what is reported in the literatures (Ref 30). It was reported previously (Ref 28) by us that the dispersoids were quite stable at 1223 K retaining their nanocrystallinity with a size range of 2–14 nm, even in a model alloy and similar stability of the dispersoids are expected here.

3.3.2 Microstructural Analysis by Transmission Electron Microscopy. To shed more light on the microstructural stability displayed by the sample, as seen via EBSD analysis, further investigation through TEM is carried out and discussion is made herewith.

Figure 4(a) shows the TEM Bright Field (BF) micrograph of N&T sample exhibiting a finer microstructure. Owing to a small

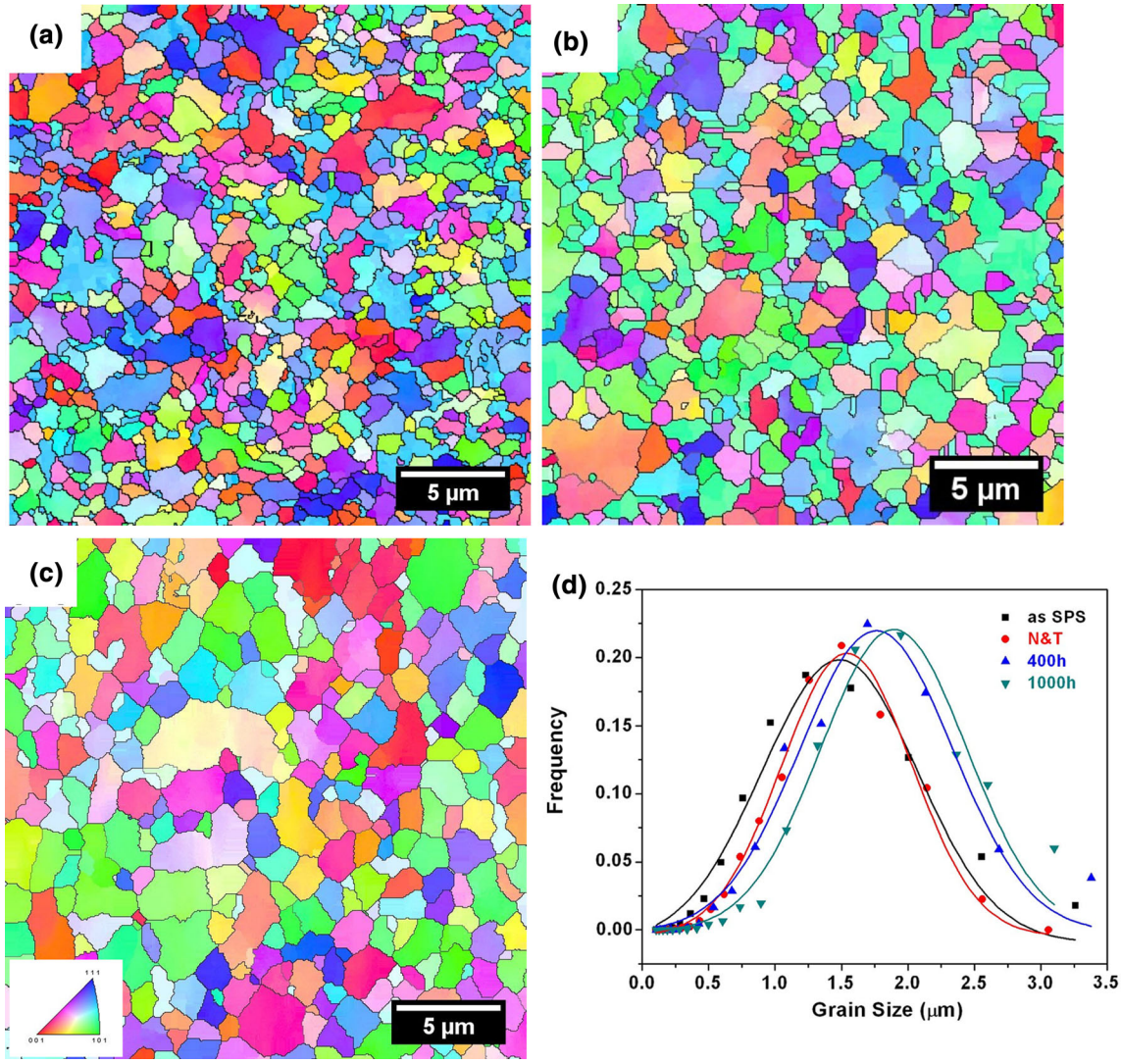

Fig. 3 EBSD Inverse Pole Figure map superimposed with grain boundary ($> 10°$) of 9 Cr ZrO_2 ODS under different thermal exposure sequences. (a) Normalized and Tempered, (b) Normalized and Tempered and 400 h aged and (c) Normalized and Tempered and 1000 h aged specimen, and (d) comparative grain size distribution map

quantity of carbon ($\sim$ 0.01 wt.%), the martensitic structure is not obviously seen, but only finer martensitic lath features are revealed, which are marked in the figure. Figure 4(b) shows the BF micrograph at a higher magnification, showing uniformly distributed nano-dispersoids. Further, the microstructure of long-term aged samples is also investigated and shown in the figure. Figure 4(c) and (d) displays the BF micrographs that correspond to N&T + 400 h aged sample at low and high magnifications, respectively. A matrix with equiaxed grains, in line with the EBSD analysis, is observed here also. The nano-features, as seen in from a grain interior in Fig. 4(d), show the retention of fine nature of these features. The results are incessant with 1000 h aged samples also, and shown in Fig. 4(e) and (f), wherein the inset shows the SAED pattern, confirming the matrix and dispersed phase. Further, the quantification of nano-dispersoids in the materials is carried out and the results are summarized in Fig. 4(g), which shows a dispersoid size distribution histogram including the size distribution for as-SPS sample. It was observed that the peak of the size distribution chart is shifting slightly toward a higher size from N&T to 1000 h. with a slight difference in the maximum value which varies from 13 nm in-as SPS to 22 nm in 1000 h aged sample. It is quite evident from the figure that the dispersoids retain their fine structure throughout the annealing duration with an average size varying from $\sim$ 4 nm in the as SPS sample to $\sim$ 7 nm after 1000 h aging, exhibiting extraordinary stability by the dispersoids. Additionally, the normal distribution to the histogram is also plotted and shown in the graph, which reveals that, the distribution of sizes is relatively narrower for the as-SPS sample in comparison with 400 and 1000 h aged samples. It is to be mentioned here that in as milled condition, the dispersoids possess a size distribution

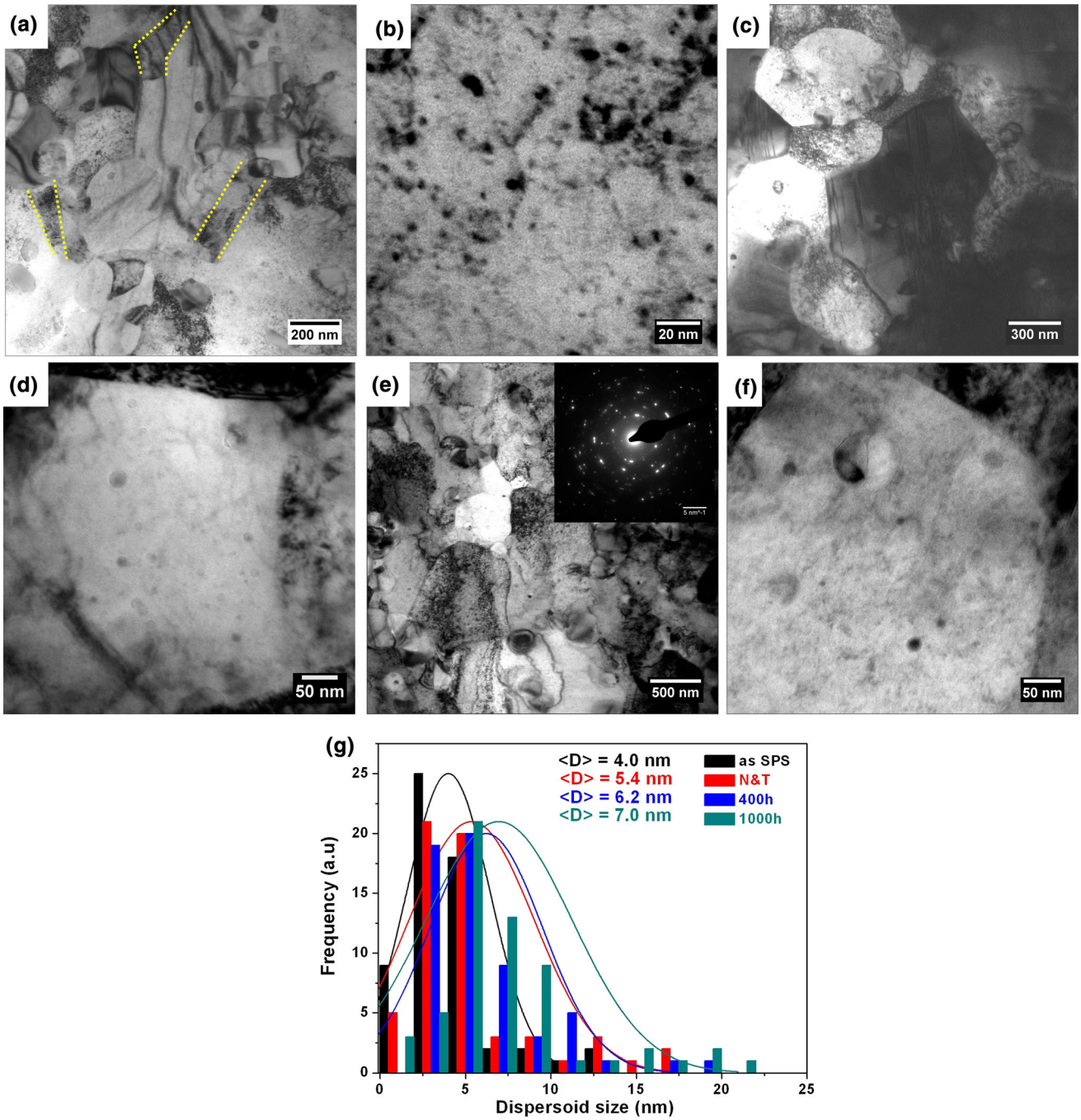

Fig. 4 (a) & (b) TEM Bright Field micrographs of Normalized and Tempered ZrO_2 ODS steel. (c)&(d) TEM Bright Field micorgraphs of Normalized and Tempered and 400 h aged ZrO_2 ODS steel. (e)&(f) TEM Bright Field micorgraphs of Normalized and Tempered and1000h aged ZrO_2 ODS steel. (g) Dispersoids size distribution histogram for as SPS, Normalized and Tempered and 400 and 1000 h aged samples

which varies from 2 to 12 nm, as reported by us previously (Ref 26) and current results show the dispersoid sizes not varying drastically from this size distribution indicating its superior stability. The value of dispersoid sizes also compares well with the reported values in the literature in a similar system. Zheng et al. (Ref 51) reported a dispersoid size of 6.9 nm after consolidation, which increased only slightly to 8.1 nm after 10000 h aging at 973 K. Here as well, the maximum size of dispersoids was limited to $\sim$ 20 nm, in close agreement to present work. In an another study (Ref 50), Y_2O_3 size was reported to be 9.2 nm, immediately after sintering,

Table 3 Vickers hardness values of the various samples with 50 g load

Sl. No	Sample ID	Hardness, $HV_{0.05}$
1	ZrO_2 ODS: as SPS	479 ± 79
2	ZrO_2 ODS: N&T	402 ± 26
3	ZrO_2 ODS: 400 h	378 ± 22
4	ZrO_2 ODS: 1000 h	374 ± 20

which increased to 12 nm after annealing at 1073 K, once again in the same size range as reported here.

3.4 Evaluation of Mechanical Property of 9Cr ZrO_2 ODS Steel

3.4.1 Hardness Measurements. The microstructural analysis as discussed earlier indicated at a stable microstructure with ultrafine grains and high-density of nano-scale oxides. Attempts are made here to correlate the observed behavior to mechanical properties through Vickers Hardness measurements. Table 3 shows the variation of hardness for 9Cr ZrO_2 ODS steel under different conditions. A hardness value of $\sim$ 479 $HV_{0.05}$ is observed in as SPS sample, which decreased to $\sim$ 402 $HV_{0.05}$ after N&T. Further, the hardness shows a little dip in going from N&T to 400 h aged, but shows saturation from 400 to 1000 h aging. The steep decrease in hardness from as SPS to normalizing and tempering is understood in terms of annihilation of dislocations in the material during the thermal exposure, mainly taking place during the initial hours. This is expected, as the ball milling is known to induce high amount of dislocations (Ref 29) and there will be insufficient time during consolidation through SPS for relaxation of these excess strain and consequently, strain relieving through dislocation annihilation takes place during the Normalizing and Tempering treatment and corresponding decrease in hardness is expected. The hardness values are reported in the literature for various ODS systems in summarized in Table 4 along with the values from this work. The observed spread of hardness values in the table is understood as due to the varying chemistry, process conditions and thermomechanical treatment sequences in these materials. Further, the saturation of hardness from 400 to 1000 h is also consistent with the comparable grain sizes and dispersoid sizes at these conditions, essentially indicating at a stable microstructure and it is in line with reported data on similar system. Zheng et al. reported a hardness value of 382 HV for a 9Cr ODS system, after 10000 h aging at 973 K (Ref 51). The retention of a high hardness value even after a long-term thermal exposure at 973 K is promising and expected to be beneficial from its practical application point of view.

3.4.2 Estimation of Yield Strength. To understand the strengthening behavior in the 9Cr ZrO_2 ODS steel due to the contribution from dispersoids and fine grains, the microstructural details discussed so far are utilized and arrived at an estimation of yield stress. The yield stress at room temperature may be estimated from the equation; (Ref 53),

$$\sigma_y = \sigma_m + \sigma_d + \sigma_i \quad \text{(Eq 1)}$$

where, $\sigma_m$is the matrix yield stress, σ_d is the direct strengthening due to the dispersoids or nano-clusters, and σ_i is the indirect strengthening due to the Hall–Petch effect. The direct strengthening due to dispersoids may be written as (Ref 53),

$$\sigma_d = \frac{MGb}{d_p}\left[\frac{6f}{\pi}\right]^{1/2} \quad \text{(Eq 2)}$$

where, M, G, b are Taylor factor, shear modulus and the Burgers vector, respectively. The strengthening due to dispersoids can be estimated with an input from the volume fraction f of the dispersoids and its diameter, d_p. The indirect strengthening due to grain size is also known as Hall–Petch strengthening and can be calculated from,

$$\sigma_i = k \times d^{-1/2} \quad \text{(Eq 3)}$$

where k is a Hall–Petch constant and d is the grain size.

Using the above formulas, the analysis of yield stress is carried out for N&T, N&T + 400 h and N&T + 1000 h samples. The grain size and average dispersoid diameter are obtained from the EBSD and TEM investigations, as discussed earlier. The other material-related parameters for the calculation of yield stress are taken from literature and listed in Table 5.

The various contributions for strengthening in 9Cr ZrO_2 ODS are evaluated using the above parameters and summarized in Fig. 5.

It can be observed from the above graph that the major contribution for yield strength of 9Cr ZrO_2 ODS steels comes mainly from dispersoids. The finer grain size also contributes substantially to the yield strength thanks to SPS. The calculated yield stress mentioned in the above graph is obtained by using the numerical relation that yield stress = 3*Vickers Hardness (Ref 54). A good correlation between measured and calculated values is obtained. The superior strength of the alloy at room temperature and a large contribution of strength from dispersoids indicate at a superior strength at elevated temperatures because dispersoids in ODS steels can suppress the dislocation movement, as well as inhibit the grain boundary migration through pinning. Thus, it is expected that material shows superior properties even at high temperatures. In order to assess the material in comparison with existing ODS systems, the literature reported Yield Strength values are compared and shown in Table 4. The observed variations in Yield Strength values in various systems are due to the varying chemistry, processing condition and thermomechanical treatment sequence, similar to the hardness values. However, when compared with material systems with similar processing and heat treatment sequences, the Yield Strength values were in fairly good agreement (Ref 55, 56).

4. Conclusions

- The consolidation of 9Cr ZrO_2 ODS powder through SPS is carried out, and a specimen of $\sim$ 94% density is obtained.
- Microstructure of as-SPS sample characterized through SEM/EBSD and TEM revealed a fine-grained morphology with the presence of dislocations indicating strained microstructure.
- The studies on N&T and high-temperature long-term aged specimens indicated an excellent stability of the microstructure with retention of fine-grained structure and dispersoids.
- The mechanical properties are measured through Vickers Hardness and correlated with Yield stress. The Yield stress is also calculated through predictive tools, and a good correlation between the two is observed. Major contributor to strength was proved to be dispersoids, with a substantial contribution from fine grains.
- The stable microstructure with fine grains, stable dispersoids and high strength, indicates at promising high temperature properties of the material, thus validating the superiority of 9Cr ZrO_2 ODS.

Table 4 The reported values for Hardness and Yield Strength in various ODS steel systems

Sample	Processing condition	Hardness	Yield Strength (MPa)	Refs
9 Cr ZrO_2 ODS	As SPS	479 HV	1437	Present work
	SPS + N&T@1050 °C, 1 h	402 HV	1206	
	SPS + N&T + 400 °C, 400 h	378 HV	1134	
	SPS + N&T + 400 °C, 1000 h	374 HV	1122	
16MnV—0.5 wt.% ZrO_2 steel	As cast	…	415 ± 4	(Ref 57)
	Quenched	…	859 ± 5	
	Normalized	…	493 ± 6	
Q345—0.5 wt.% ZrO_2 steel	As cast	4.87 GPa	…	(Ref 58)
	Quenched	5.26 GPa	…	
	Normalized	4.93 GPa	…	
21Cr—0.3 wt.% Y_2O_3 Austenitic ODS	Hot Pressed	…	466	(Ref 59)
21Cr—0.3 wt.% ZrO_2 Austenitic ODS	Hot Pressed	…	419	
21Cr—0.15 wt.% Y_2O_3—0.15 wt.% ZrO_2 Austenitic ODS	Hot Pressed	…	494	
9Cr- 0.35wt.% Y_2O_3 ODS	Sintered Bulk ODS steel	433 HV	…	(Ref 50)
	Annealed Bulk ODS steel	271 HV	…	
12 Cr—0.2wt.% Y_2O_3 ODS	As HIP	6.46 GPa	…	(Ref [60])
	HIP + 1 h annealing at 1150 °C	3.89 Gpa	…	
25Cr-0.5wt.% ZrO_2 ODS steel	sintered	142.8 HV	…	(Ref 61)
21 Cr duplex ODS steel with La_2O_3 dispersoid	SPS	739 ± 9.1 HV	…	(Ref 62)
14Cr-0.35wt.% Y_2O_3 ODS steel	HIP	431 ± 6 HV	…	(Ref 63)
14Cr-0.35wt.% Y_2O_3–0.3 wt.% Zr ODS steel		552 ± 9 HV	…	
12Cr–0.22 wt.% Y_2O_3 ODS	Hot Extruded and 1150°C_1h annealed	3.4 GPa	991 MPa	(Ref 55)
12Cr–0.25 wt.% Y_2O_3 ODS RAF steel	SPS	5.5 GPa (HV0.1)	…	(Ref 56)
		5.75 GPa (nanoindentation)	…	
14Cr-0.25wt.% Y_2O_3 ODS steel	SPS	~ 320 HV*	…	(Ref 64) *Data retrieved from graph
14Cr-0.25wt.% Y_2O_3 ODS steel (Boron added)		~ 340 HV*	…	
14Cr-1.62 wt.% Y–Ti-Zr-O ODS steel		~ 410 HV*	…	
14Cr-1.97 wt.% Y–Ti-Zr-O ODS steel (Boron added)		~ 400 HV*	…	
14Cr-0.3wt.% Y_2O_3 ODS steel (GETMAT)	Hot Extruded and 1150°C_1.5 h annealed	392 ± 4 $HV_{0.1}$	…	(Ref 65)
20Cr-0.5wt.% Y_2O_3 ODS steel (PM 2000)	Hot Extruded	332 HV	…	(Ref 66)
14Cr-0.3wt.% Y_2O_3 ODS steel	HIP + 900°C_1h annealed + High speed hydrostatic extrusion	460 $HV_{0.1}$	…	(Ref 67)
9Cr-0.37 wt.% Y_2O_3 ODS steel	Hot Extruded, N&T at 1050°C_1h and 800°C_ 1 h	389 ± 2 $HV_{0.2}$	…	(Ref 51)
	• Before aging	386 ± 1 $HV_{0.2}$		
	• 100 h @ 700 °C	382 ± 2 $HV_{0.2}$		
	• 10000 h @ 700 °C			
9Cr ODS steel	Hot Pressed	6.49 ± 0.12 GPa	1791 ± 35	(Ref 68)
9Cr-1Hf ODS steel		7.08 ± 0.12 GPa	2449 ± 48	
14Cr-0.3wt.% Y_2O_3 ODS steel	Hot Extruded	447 ± 5 $HV_{0.1}$	…	(Ref 69)
14Cr-0.3wt.% Y_2O_3 ODS steel	SPS	850 HV	…	(Ref 70)

Table 5 The material constants used in the estimation of yield stress

Parameter	Value	Refs.
Taylor factor, M	3.06	(Ref 53)
Shear modulus, G	80 GPa	(Ref 53)
Burgers vector, b	0.248 nm	(Ref 53)
Hall Petch constant, k	0.2 MPa $m^{1/2}$	(Ref 71)

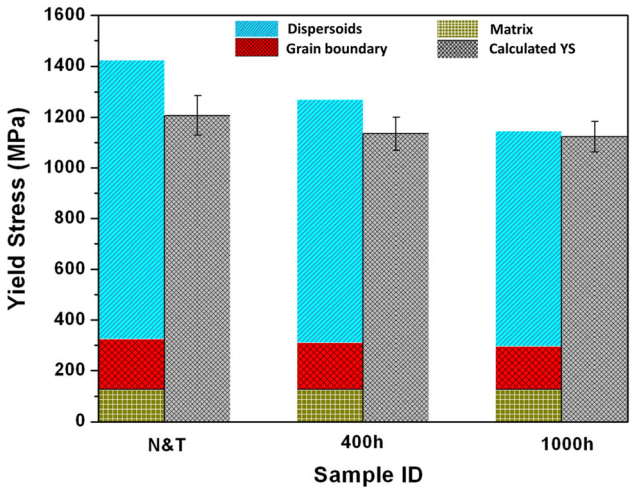

Fig. 5 Comparison of measured and calculated yield stress along with various contributions to strengthening

Acknowledgments

The authors acknowledge the UGC-DAE-CSR, Kokilamedu for providing the extended Helios NanoLab—600i facility for SEM characterization. One of the authors, RKG, acknowledges Department of Atomic Energy, India, for fellowship and thank Dr. Manmath Kumar Dash, University of Birmingham, for his help during EBSD experiments.

Funding

Open access funding provided by Manipal Academy of Higher Education, Manipal.

Conflict of interest

The authors declare that they have no known competing financial interests or personal relationships that could have appeared to influence the work reported in this paper.

References

1. S.J. Zinkle and G.S. Was, Materials Challenges in Nuclear Energy, *Acta Mater.*, 2013, **61**(3), p 735–758
2. B. Raj, M. Vijayalakshmi, P.R. Vasudeva Rao and K.B.S. Rao, Challenges in Materials Research for Sustainable Nuclear Energy, *MRS Bull. Mater. Res. Soc.*, 2008, **33**(4), p 327–337
3. S. Saroja, A. Dasgupta, R. Divakar, S. Raju, E. Mohandas, M. Vijayalakshmi, K. Bhanu Sankara Rao and B. Raj, Development and Characterization of Advanced 9Cr Ferritic/Martensitic Steels for Fission and Fusion Reactors, *J. Nucl. Mater.*, 2011, **409**(2), p 131–139
4. D. Srivastava, K. Kapoor and G. Amarendra, Development of Advanced Nuclear Structural Materials for Sustainable Energy Development, *J. Indian Inst. Sci.*, 2022, **102**(1), p 391–404. https://doi.org/10.1007/s41745-022-00287-z
5. G.K. Dey, Structural Materials in Nuclear Energy Sector, *Future Landscape of Structural Materials in India*. Springer, London, 2022, p 59–77
6. A. Couet, Integrated High-Throughput Research in Extreme Environments Targeted toward Nuclear Structural Materials Discovery, *J. Nucl. Mater.*, 2022, **559**, p 153425. https://doi.org/10.1016/j.jnucmat.2021.153425
7. S. Ukai and M. Fujiwara, Perspective of ODS Alloys Application in Nuclear Environments, *J. Nucl. Mater.*, 2002, **307–311**, p 749–757. https://doi.org/10.1016/S0022-3115(02)01043-7
8. S.J. Zinkle and J.T. Busby, Structural Materials for Fission & Fusion Energy, *Mater. Today*, 2009, **12**(11), p 12–19
9. F. Bergner, I. Hilger, J. Virta, J. Lagerbom, G. Gerbeth, S. Connolly, Z. Hong, P.S. Grant and T. Weissgärber, Alternative Fabrication Routes toward Oxide-Dispersion-Strengthened Steels and Model Alloys, *Metall. Mater. Trans. A*, 2016, **47**(11), p 5313–5324. https://doi.org/10.1007/s11661-016-3616-2
10. D. Pazos, A. Cintins, V. de Castro, P. Fernández, J. Hoffmann, W.G. Vargas, T. Leguey, J. Purans, A. Anspoks, A. Kuzmin, I. Iturriza and N. Ordás, ODS Ferritic Steels Obtained from Gas Atomized Powders through the STARS Processing Route: Reactive Synthesis as an Alternative to Mechanical Alloying, *Nucl. Mater. Energy*, 2018, **17**, p 1–8. https://doi.org/10.1016/j.nme.2018.06.014
11. M.B. Wilms, N. Pirch and B. Gökce, Manufacturing Oxide-Dispersion-Strengthened Steels Using the Advanced Directed Energy Deposition Process of High-Speed Laser Cladding, *Prog. Addit. Manuf.*, 2022 https://doi.org/10.1007/s40964-022-00319-1
12. D. Zhang, J.T. Darsell, J. Wang, X. Ma, G.J. Grant, I.E. Anderson, J.R. Rieken, D.J. Edwards, W. Setyawan, T.J. Horn and G.R. Odette, No Ball Milling Needed: Alternative ODS Steel Manufacturing with Gas Atomization Reaction Synthesis (GARS) and Friction-Based Processing, *J. Nucl. Mater.*, 2022, **566**, p 153768. https://doi.org/10.1016/j.jnucmat.2022.153768
13. Y. Zhuang, X. Zhang, T. Peng, H. Fan, X. Zhang, Q. Yan and A.A. Volinsky, Effects of Yttrium Oxides on the Microstructure and Mechanical Properties of 15–15Ti ODS Alloy Fabricated by Casting, *Mater. Charact.*, 2020, **162**, p 110228. https://doi.org/10.1016/j.matchar.2020.110228
14. P.K. Parida, A. Dasgupta, K. Jayasankar, M. Kamruddin and S. Saroja, Structural Studies of Y_2O_3 Dispersoids during Mechanical Milling and Annealing in a Fe-15 Y_2O_3 Model ODS Alloy, *J. Nucl. Mater.*, 2013, **441**(1–3), p 331–336
15. P.K. Parida, A. Dasgupta, K. Jayasankar, M. Kamruddin and S. Saroja, Structural Studies of Y_2O_3 Dispersoids during Mechanical Milling and Annealing in a Fe-15 Y_2O_3 Model ODS Alloy, *J. Nucl. Mater.*, 2013, **441**(1), p 331–336. https://doi.org/10.1016/j.jnucmat.2013.06.016
16. P.K. Parida, A. Dasgupta, K.G. Raghavendra, K. Jayasankar and S. Saroja, Structural Studies of Dispersoids in Fe–15 wt.% Y_2O_{3-5} wt.% Ti Model ODS Alloys During Milling and Subsequent Annealing, *Trans. Indian Inst. Met.*, 2017, **70**(6), p 1409–1415. https://doi.org/10.1007/s12666-016-0911-y

17. I. Monnet, T. Van den Berghe and Ph. Dubuisson, A Comparison between Different Oxide Dispersion Strengthened Ferritic Steel Ongoing in Situ Oxide Dissolution in High Voltage Electron Microscope, *J. Nucl. Mater.*, 2012, **424**(1–3), p 204–209
18. L. Li, W. Xu, M. Saber, Y. Zhu, C.C. Koch and R.O. Scattergood, Influence of Scandium Addition on the High-Temperature Grain Size Stabilization of Oxide-Dispersion-Strengthened (ODS) Ferritic Alloy, *Mater. Sci. Eng. A*, 2015, **636**, p 565–571
19. W.Z. Xu, L.L. Li, M. Saber, C.C. Koch, Y.T. Zhu and R.O. Scattergood, Nano ZrO_2 Particles in Nanocrystalline Fe-14Cr-1.5Zr Alloy Powders, *J. Nucl. Mater.*, 2014, **452**(1–3), p 434–439
20. S. Pasebani and I. Charit, Effect of Alloying Elements on the Microstructure and Mechanical Properties of Nanostructured Ferritic Steels Produced by Spark Plasma Sintering, *J. Alloys Compd.*, 2014, **599**, p 206–211. https://doi.org/10.1016/j.jallcom.2014.01.243
21. S. Pasebani, I. Charit, Y.Q. Wu, D.P. Butt and J.I. Cole, Mechanical Alloying of Lanthana-Bearing Nanostructured Ferritic Steels, *Acta Mater.*, 2013, **61**(15), p 5605–5617
22. J. Hoffmann, M. Rieth, R. Lindau, M. Klimenkov, A. Möslang and H.R.Z. Sandim, Investigation on Different Oxides as Candidates for Nano-Sized ODS Particles in Reduced-Activation Ferritic (RAF) Steels, *J. Nucl. Mater.*, 2013, **442**(1–3), p 444–448
23. Y. Wu, H. Zhao, J. Li, Y. Zhang and T. Liu, Effects of $Y_4Zr_3O_{12}$ Addition on the Microstructure and Mechanical Properties of Fe–15Cr–2W-0.35Ti ODS Steels, *Mater. Sci. Eng. A*, 2021, **804**, p 140734. https://doi.org/10.1016/j.msea.2021.140734
24. A. Kumar, B. Jayabalan, C. Singh, J. Jain, S. Mukherjee, K. Biswas and S.S. Singh, Role of Chromium Content on the Microstructure and Mechanical Properties of Lanthana Based Ferritic ODS Steels, *Met. Mater. Int.*, 2022 https://doi.org/10.1007/s12540-022-01278-6
25. G.N. Kaushik, M. Nagini, M.S.P. Reddy, N.Y. Hebalkar, R. Vijay and B.S. Murty, Effect of Zr and ZrO_2 on Aqueous Corrosion Behaviour of Oxide Dispersion Strengthened 9Cr Ferritic-Martensitic Steels, *Mater. Lett.*, 2022, **324**, p 132428. https://doi.org/10.1016/j.matlet.2022.132428
26. K.G. Raghavendra, A. Dasgupta, C. Ghosh, K. Jayasankar, V. Srihari and S. Saroja, Development of a Novel ZrO_2 Dispersion Strengthened 9Cr Ferritic Steel: Characterization of Milled Powder and Subsequent Annealing Behavior, *Powder Technol.*, 2018, **327**, p 267–274. https://doi.org/10.1016/j.powtec.2017.12.076
27. A. García-Junceda, N. García-Rodríguez, M. Campos, M. Cartón-Cordero and J.M. Torralba, Effect of Zirconium on the Microstructure and Mechanical Properties of an Al-Alloyed ODS Steel Consolidated by FAHP, *J. Am. Ceram. Soc.*, 2015, **98**(11), p 3582–3587. https://doi.org/10.1111/jace.13691
28. K.G. Raghavendra, A. Dasgupta, R.N. Hajra, K. Jayasankar, V. Srihari and S. Saroja, Thermal Evolution of Fe-ZrO_2 Nanocomposite: Insights from Calorimetric and Microscopy Investigations, *Mater. Charact.*, 2017, **132**, p 448–457. https://doi.org/10.1016/j.matchar.2017.09.010
29. K.G. Raghavendra, A. Dasgupta, P. Bhaskar, K. Jayasankar, C.N. Athreya, P. Panda, S. Saroja, V. Subramanya Sarma and R. Ramaseshan, Synthesis and Characterization of Fe-15 wt.% ZrO_2 Nanocomposite Powders by Mechanical Milling, *Powder Technol.*, 2016, **287**, p 190–200. https://doi.org/10.1016/j.powtec.2015.10.003
30. H. Xu, Z. Lu, D. Wang and C. Liu, Microstructure Refinement and Strengthening Mechanisms of a 9Cr Oxide Dispersion Strengthened Steel by Zirconium Addition, *Nucl. Eng. Technol.*, 2017, **49**(1), p 178–188. https://doi.org/10.1016/j.net.2017.01.002
31. H. Xu, Z. Lu, D. Wang and C. Liu, Effect of Zirconium Addition on the Microstructure and Mechanical Properties of 15Cr-ODS Ferritic Steels Consolidated by Hot Isostatic Pressing, *Fusion Eng. Des.*, 2017, **114**, p 33–39. https://doi.org/10.1016/j.fusengdes.2016.11.011
32. P. Song, D. Morrall, Z. Zhang, K. Yabuuchi and A. Kimura, Radiation Response of ODS Ferritic Steels with Different Oxide Particles under Ion-Irradiation at 550 °C, *J. Nucl. Mater.*, 2018, **502**, p 76–85
33. C.P. Massey, P.D. Edmondson, K.A. Unocic, Y. Yang, S.N. Dryepondt, A. Kini, B. Gault, K.A. Terrani and S.J. Zinkle, The Effect of Zr on Precipitation in Oxide Dispersion Strengthened FeCrAl Alloys, *J. Nucl. Mater.*, 2020, **533**, p 152105. https://doi.org/10.1016/j.jnucmat.2020.152105
34. S. Peng, Z. Lu and L. Yu, Control of Microstructure and Hardness of ODS-CrFeNi MEAs by Y_2O_3/Zr Addition, *Mater. Charact.*, 2022, **186**, p 111816. https://doi.org/10.1016/j.matchar.2022.111816
35. X. Wang, Z. Lu, Z. Li, Y. Shi and H. Xu, Effect of Zr Content on Microstructure and Hardness of ODS-FeCrAl Alloys, *Mater. Charact.*, 2022, **192**, p 112221. https://doi.org/10.1016/j.matchar.2022.112221
36. X. Zhou, G. Li, X. Shen and Y. Liu, Tensile Strength Improvement of Martensitic ODS Steels with Zr and Hf Additions, *Mater. Sci. Eng. A.*, 2022, **829**, p 142071. https://doi.org/10.1016/j.msea.2021.142071
37. P. Song, A. Kimura, K. Yabuuchi, P. Dou, H. Watanabe, J. Gao and Y.-J. Huang, Assessment of Phase Stability of Oxide Particles in Different Types of 15Cr-ODS Ferritic Steels under 6.4 MeV Fe Ion Irradiation at 200 °C, *J. Nucl. Mater.*, 2020, **529**, p 151953
38. A.N. Velikodnyi, V.N. Voyevodin, A.S. Kalchenko, S.A. Karpov, I.V. Kolodiy, M.A. Tikhonovsky, G.D. Tolstolutskaya and F.A. Garner, Impact of Nano-Oxides and Injected Gas on Swelling and Hardening of 18Cr10NiTi Stainless Steel during Ion Irradiation, *J. Nucl. Mater.*, 2022, **565**, p 153666
39. P.K. Parida, A. Dasgupta and S.K. Sinha, Comparison of Microstructure and Microtexture Evolution in 9Cr and 18Cr Oxide Dispersion-Strengthened Steels during Fuel Clad Tube Fabrication, *J. Mater. Eng. Perform.*, 2021, **30**(12), p 9227–9236. https://doi.org/10.1007/s11665-021-06108-1
40. I. Hilger, F. Bergner, A. Ulbricht, A. Wagner, T. Weißgärber, B. Kieback, C. Heintze and C.D. Dewhurst, Investigation of Spark Plasma Sintered Oxide-Dispersion Strengthened Steels by Means of Small-Angle Neutron Scattering, *J. Alloys Compd.*, 2016, **685**, p 927–935
41. Y. Chang, D. Huang, C. Jia, C. Ge, D. Liang and P. Gao, Oxide Dispersion Strengthened Ferritic Steel Fabricated by Mechanical Alloying and Spark Plasma Sintering, *Powder Metall.*, 2014, **57**(2), p 103–110
42. C. Lu, Z. Lu, R. Xie, C. Liu and L. Wang, Microstructure of HIPed and SPSed 9Cr-ODS Steel and Its Effect on Helium Bubble Formation, *J. Nucl. Mater.*, 2016, **474**, p 65–75
43. J. Yang, Z.M. Guo, W.W. Yang, J. Luo and C.G. Chen, Microstructure and Mechanical Properties of 9Cr-ODS Ferritic/Martensitic Steels by Mechanically Alloyed and Spark Plasma Sintering, *Mater. Sci. Forum*, 2013, **747–748**, p 636–640
44. K.N. Allahar, J. Burns, B. Jaques, Y.Q. Wu, I. Charit, J. Cole and D.P. Butt, Ferritic Oxide Dispersion Strengthened Alloys by Spark Plasma Sintering, *J. Nucl. Mater.*, 2013, **443**(1–3), p 256–265
45. C. Heintze, M. Hernández-Mayoral, A. Ulbricht, F. Bergner, A. Shariq, T. Weissgärber and H. Frielinghaus, Nanoscale Characterization of ODS Fe-9%Cr Model Alloys Compacted by Spark Plasma Sintering, *J. Nucl. Mater.*, 2012, **428**, p 139–146
46. M.S. Staltsov, I.I. Chernov, I.A. Bogachev, B.A. Kalin, E.A. Olevsky, L.J. Lebedeva and A.A. Nikitina, Optimization of Mechanical Alloying and Spark-Plasma Sintering Regimes to Obtain Ferrite–Martensitic ODS Steel, *Nucl. Mater. Energy*, 2016, **9**, p 360–366
47. R. Xie, Z. Lu, C. Lu, Z. Li, X. Ding and C. Liu, Microstructures and Mechanical Properties of 9Cr Oxide Dispersion Strengthened Steel Produced by Spark Plasma Sintering, *Fusion Eng. Des.*, 2017, **115**, p 67–73. https://doi.org/10.1016/j.fusengdes.2016.12.034
48. A. Meza, E. Macía, A. García-Junceda, L.A. Díaz, P. Chekhonin, E. Altstadt, M. Serrano, M.E. Rabanal and M. Campos, Development of New 14 Cr ODS Steels by Using New Oxides Formers and B as an Inhibitor of the Grain Growth, *Metals (Basel)*, 2020, **10**(10), p 1344. https://doi.org/10.3390/met10101344
49. Z. Li, L. Chen, H. Zhang, S. Zhang and Z. Zhang, Effect of Annealing Temperature on Microstructure and Mechanical Properties in Oxide Dispersion Strengthened Fe-14Cr Alloys Prepared by Spark Plasma Sintering, *Mater. Res. Exp.*, 2019, **6**(12), p 126515. https://doi.org/10.1088/2053-1591/ab52c3
50. X. Zhou, Y. Liu, L. Yu, Z. Ma, Q. Guo, Y. Huang and H. Li, Microstructure Characteristic and Mechanical Property of Transformable 9Cr-ODS Steel Fabricated by Spark Plasma Sintering, *Mater. Des.*, 2017, **132**, p 158–169. https://doi.org/10.1016/j.matdes.2017.06.063
51. P. Zheng, Y. Li, J. Zhang, J. Shen, T. Nagasaka, T. Muroga and H. Abe, On the Thermal Stability of a 9Cr-ODS Steel Aged at 700 °C up to 10000 h-Mechanical Properties and Microstructure, *Mater. Sci. Eng. A.*, 2020, **783**, p 139292. https://doi.org/10.1016/j.msea.2020.139292
52. Y. Li, H. Abe, F. Li, Y. Satoh, Y. Matsukawa, T. Matsunaga and T. Muroga, Grain Structural Characterization of 9Cr–ODS Steel Aged at 973K up to 10,000h by Electron Backscatter Diffraction, *J. Nucl. Mater.*, 2014, **455**(1), p 568–572. https://doi.org/10.1016/j.jnucmat.2014.08.047

53. J.H. Schneibel, M. Heilmaier, W. Blum, G. Hasemann and T. Shanmugasundaram, Temperature Dependence of the Strength of Fine- and Ultrafine-Grained Materials, *Acta Mater.*, 2011, **59**(3), p 1300–1308
54. K. Rajan, V.S. Sarma, T.R.G. Kutty and B.S. Murty, Hot Hardness Behaviour of Ultrafine Grained Ferritic Oxide Dispersion Strengthened Alloys Prepared by Mechanical Alloying and Spark Plasma Sintering, *Mater. Sci. Eng. A*, 2012, **558**, p 492–496. https://doi.org/10.1016/j.msea.2012.08.033
55. M. Frelek-Kozak, L. Kurpaska, M. Lesniak, I. Jozwik and J. Jagielski, Mechanical and Structural Properties of ODS RAF Steels Submitted to Low-Energy Ions Irradiation, *Fusion Eng. Des.*, 2018, **127**, p 54–59
56. M. Frelek-Kozak, L. Kurpaska, E. Wyszkowska, J. Jagielski, I. Jozwik and M. Chmielewski, Evaluation of Consolidation Method on Mechanical and Structural Properties of ODS RAF Steel, *Appl. Surf. Sci.*, 2018, **446**, p 215–221. https://doi.org/10.1016/j.apsusc.2018.01.163
57. B.A. Wang, N. Wang, Y.J. Yang, H. Zhong, M.Z. Ma, X.Y. Zhang and R.P. Liu, Microstructure and Mechanical Properties of ZrO_2 Particle Dispersion Strengthened 16MnV Steel, *Mater. Sci. Eng., A*, 2017, **692**, p 168–173. https://doi.org/10.1016/j.msea.2017.03.072
58. B. Wang, N. Wang, Y. Yang, H. Zhong, M. Ma, X. Zhang and R. Liu, Fabrication, Microstructures and Mechanical Properties of ZrO2 Dispersion-Strengthened Q345 Steel, *Trans. Nonf. Metals Soc. China*, 2018, **28**(6), p 1132–1140. https://doi.org/10.1016/S1003-6326(18)64750-8
59. P.K. Kumar, N.V. Sai and A.G. Krishna, Effect of Y2O3 and ZrO2 on the Microstructure and Mechanical Properties of Nano-ODS 21Cr-9Mn-6Ni Steels, *Mater. Tehnol.*, 2018, **52**(4), p 493–497
60. K. Nowik and Z. Oksiuta, Microstructure, Grain Growth and Hardness of Nanostructured Ferritic ODS Steel Powder during Annealing, *Metall. Microst. Anal.*, 2021, **10**(3), p 355–366. https://doi.org/10.1007/s13632-021-00746-6
61. M. Silalahi, B. Bandriyana, S. Ahda, B. Sugeng and A. Dimyati, Synthesis and Characterization of High Chromium Zirconiaoxide Dispersion Strengthened (ODS) Steel, *J. Phys. Conf. Ser.*, 2020, **1436**(1), p 012055
62. A. Kumar, B. Jayabalan, C. Singh, J. Jain, S. Mukherjee, K. Biswas and S.S. Singh, Processing and Properties of Yttria and Lanthana Dispersed ODS Duplex Stainless Steels, *Mater. Sci. Eng. A*, 2022, **837**, p 142746
63. W. Li, H. Xu, X. Sha, J. Meng and Z. Wang, Microstructure and Mechanical Properties of 14Cr-ODS Steels with Zr Addition, *High Temp. Mater. Processes (London)*, 2019, **2019**(38), p 404–410
64. A. Meza, E. Macía, A. García-Junceda, L.A. Díaz, P. Chekhonin, E. Altstadt, M. Serrano, M.E. Rabanal and M. Campos, Development of New 14 Cr ODS Steels by Using New Oxides Formers and B as an Inhibitor of the Grain Growth, *Metals (Basel)*, 2020, **10**(10), p 1344
65. A. García-Junceda, M. Hernández-Mayoral and M. Serrano, Influence of the Microstructure on the Tensile and Impact Properties of a 14Cr ODS Steel Bar, *Mater. Sci. Eng. A*, 2012, **556**, p 696–703. https://doi.org/10.1016/j.msea.2012.07.051
66. Z.B. Zhang, N.R. Tao, O.V. Mishin and W. Pantleon, Oxide Dispersion-Strengthened Steel PM2000 after Dynamic Plastic Deformation: Nanostructure and Annealing Behaviour, *J. Mater. Sci.*, 2016, **51**(11), p 5545–5555. https://doi.org/10.1007/s10853-016-9859-x
67. Z. Oksiuta, M. Lewandowska and K.J. Kurzydłowski, Mechanical Properties and Thermal Stability of Nanostructured ODS RAF Steels, *Mech. Mater.*, 2013, **67**, p 15–24
68. B.R. Sun, A.D. Zhou, Y.L. Li, Z.L. Zhang, C.C. Du, S.X.Y. Gu, Z. Chen, X.C. Cai, S.W. Xin and T.D. Shen, Ultrafine-Grained Oxide-Dispersion-Strengthened 9Cr Steel with Exceptional Strength and Thermal Stability, *Nucl. Mater. Energy*, 2022, **30**, p 101112
69. M. De Sanctis, A. Fava, G. Lovicu, R. Montanari, M. Richetta, C. Testani and A. Varone, Mechanical Characterization of a Nano-ODS Steel Prepared by Low-Energy Mechanical Alloying, *Metals (Basel)*, 2017, **7**(8), p 11869. https://doi.org/10.3390/met7080283
70. Z. Li, L. Chen, H. Zhang, S. Zhang and Z. Zhang, Effect of Annealing Temperature on Microstructure and Mechanical Properties in Oxide Dispersion Strengthened Fe-14Cr Alloys Prepared by Spark Plasma Sintering, *Mater. Res. Exp.*, 2019, **6**(12), p 126515
71. W. Horvath, H. Hofer and E. Werner, Yield Strength of Nitrogen Alloyed Duplex Steels: Experiments and Micromechanical Predictions, *Comput. Mater. Sci.*, 1997, **9**(1–2), p 76–84